Revision 1

Topotactic and reconstructive changes at high pressure and temperatures from Cs-natrolite to Cs-hexacelsian

Huijeong Hwang,[1] Donghoon Seoung,[1] G. Diego Gatta,[2] Douglas A. Blom,[3] Thomas Vogt,[3] Yongjae Lee[1,] *

[1]Department of Earth System Sciences, Yonsei University, Seoul 120-749, Korea

[2]Dipartimento di Scienze della Terra, Università degli Studi di Milano, Via Botticelli, 23, I-20133 Milano, Italy

[3]NanoCenter & Department of Chemistry and Biochemistry, University of South Carolina, Columbia, SC 29208, USA

Abstract

Synchrotron X-ray powder diffraction experiments have been performed on dehydrated Cs-exchanged natrolite in order to systematically investigate successive transitions under high pressures and temperatures. At pressures above 0.5(1) GPa using H_2O as a pressure transmitting medium and after heating to 100 °C, dehydrated $Cs_{16}Al_{16}Si_{24}O_{80}$ (deh-Cs-NAT) transforms to a hydrated phase $Cs_{16}Al_{16}Si_{24}O_{80}{\cdot}16H_2O$ (Cs-NAT-II), which has a ca. 13.9% larger unit-cell volume. Further compression and heating to 1.5 GPa and 145 °C results in the transformation of Cs-NAT-II to $Cs_{16}Al_{16}Si_{32}O_{96}$ (anh-Cs-POL), a H_2O-free pollucite-like triclinic phase with a 15.6% smaller unit-cell volume per 80 framework oxygen atoms ($80O_f$). At pressures and temperatures of 3.7 GPa and 180 °C, a new phase $Cs_{1.547}Al_{1.548}Si_{6.452}O_{16}$ (Cs-HEX) with a hexacelsian framework forms,

which has a ca. 1.8% smaller unit-cell volume per $80O_f$. This phase can be recovered after pressure release. The structure of the recovered Cs-HEX has been refined in space group $P6_3/mcm$ with a = 5.3731(2) Å and c = 16.6834(8) Å, and also been confirmed by HAADF-STEM real space imaging. Similar to the hexacelsian feldspar (*i.e.* $BaAl_2Si_2O_8$), Cs-HEX contains Cs^+ cations which act as bridges between the upper and lower layers composed of tetrahedra and are hexa-coordinated to the upper and lower 6-membered ring windows. These pressure- and temperature-induced reactions from a zeolite to a feldspar-like material are important constraints for the design of materials for Cs^+ immobilization in nuclear waste disposal.

Keywords : Natrolite, Hexacelsian, High-pressure, Phase transition, X-ray powder diffraction, Radioactive wastes.

Introduction

Natrolite (ideally $Na_{16}Al_{16}Si_{24}O_{80}\cdot 16H_2O$, Na-NAT) is a small pore aluminosilicate mineral that has been characterized in the early 1930s as a member of the "fibrous zeolites" group, with a framework composed of T_5O_{10} tetrahedral units (Pauling 1930 and Taylor et al. 1933). Although natrolite forms in many hydrothermal environments (Klaproth, M.H. 1803), technological applications for it have been limited as its pores are small (~2.6 Å) and filled with strongly bonded Na^+-H_2O clusters (Baur et al. 1990). However, it has recently been demonstrated that after exchanging Na^+ by K^+, these ordered Na^+-H_2O cluster rearrange into disordered K^+-H_2O ones concomitant with a

~ 10% expansion of the unit-cell volume (Lee et al. 2010, 2013). Subsequently, facile ion exchange of K^+ by Rb^+-, Cs^+-, Ca^{2+}-, Sr^{2+}-, Ba^{2+}-, Cd^{2+}-, Pb^{2+}-, and Ag^+ as extra-framework cations (EFC) is possible using traditional solution exchange methods, thus defying the notion that natrolite is only a "soda-stone" (Lee et al. 2011).

Natrolite has also been shown to undergo intriguing structural changes under hydrostatic pressure. When compressed using hydrous liquids as pressure transmitting media, the unit-cell volume of natrolite expands by ca. 7% at 1 GPa while it adsorbs H_2O into its pores and forms $Na_{16}Al_{16}Si_{24}O_{80}\cdot 24H_2O$ (Lee et al. 2005). It subsequently contracts by ca. 5% at 1.2 GPa while continuing to adsorb H_2O and forms a 'super-hydrated' zeolite $Na_{16}Al_{16}Si_{24}O_{80}\cdot 32H_2O$ (Lee et al. 2005). Super-hydration in natrolite occurs *via* cooperative rotations and anti-rotations of the T_5O_{10} tetrahedral units which increase the pore H_2O content by 50% at 1 GPa and 1.2 GPa, respectively, while the framework remains intact. This has been coined "pressure-induced hydration (PIH)" and found to be a general property of the natrolite framework depending on the type of EFC being present (Gatta 2005; Seoung et al. 2013; Gatta and Lee 2014). The observed unit-cell volume expansion is inversely related to the size of the EFC: Li^+-exchanged natrolite exhibits the largest volume expansion of ca. 20.6(1)% while doubling its H_2O content near 1 GPa, whereas Rb^+-exchanged natrolite super-hydrates near 2 GPa, while undergoing only a minute unit-cell volume expansion of 0.3(1)% when doubling its H_2O content (Seoung et al. 2013). Grima et al. (2007) showed that natrolite is an auxetic zeolite, having negative Poisson's ratios and thus being able to contract perpendicular to the direction it is being compressed (Grima et al. 2007). Using density functional theory (DFT), the auxetic properties of natrolites containing monovalent EFC could be modeled

and, furthermore, it was proposed that Cs-natrolite which does not undergo any PIH (but only a volume contraction of ca. 4.8% near 0.3 GPa) transforms under pressure by the Cs^+ cations moving to neighboring channels (Kremleva et al. 2013). This volume contraction results in significant changes of the disordered Cs^+-H_2O topology within the channels as a 90° rotation of the Cs^+ ions is concomitant with a 45° rotational ordering of the H_2O ligands when compared to the low pressure Cs-NAT-I phase. In addition, the high-pressure, high-density phase, called Cs-NAT-II, is found to be about three times more compressible than Cs-NAT-I.

We have recently found that further densification can be induced by heating Cs-NAT-II. At 1.5 GPa and 145 °C, Cs-NAT-II transforms to a pollucite-related, highly dense, and H_2O-free triclinic phase with the nominal composition $CsAlSi_2O_6$. This is an irreversible phase transition going from $Cs_{16}Al_{16}Si_{24}O_{80}\cdot 16H_2O$ to $Cs_{15}Al_{15}Si_{30}O_{80}$ which involves reconstructive changes of the framework (in preparation). After pressure release, this anhydrous pollucite-related phase is recovered as a monoclinic phase. The significant heat load caused by both nuclear decay and electron self-radiation in materials containing ^{137}Cs and ^{90}Sr during the early stages of nuclear waste disposal, calls for their separation from the waste stream and will significantly increase the storage capacity of high-level nuclear waste and reduce costs while complying with regulatory requirements. Due to its chemical stability and high Cs-loading of 42.6 weight-%, the aluminosilicate pollucite ($CsAlSi_2O_6\cdot H_2O$) has been identified as a preferred nuclear waste form for Cs (Gatta et al. 2009a, 2009b, Sanchez-Valle et al. 2010). In most cases, a multi-step process starting with CsOH is used to prepare a sol which is then hydrothermally treated at temperatures close to 200 °C to end up with a dry pollucite powder (MacLaren et al.

1999).

In this paper, we report that further pressure- and heat-treatment of the triclinic pollucite-related phase results in another reconstructive phase transformation from $Cs_{15}Al_{15}Si_{30}O_{80}$ to a more silicon-rich hexacelsian-related phase with composition $Cs_{7.74}Al_{7.74}Si_{32.26}O_{80}$. We have performed combined *in situ* high-pressure and *ex situ* high-temperature synchrotron X-ray powder diffraction and high angle annular dark field scanning transmission electron microscopy (HAADF-STEM) real space imaging and established the complete pathway of the successive structural phase transformations from dehydrated Cs-exchanged natrolite (deh-Cs-NAT) *via* its hydrated high-pressure phase (Cs-NAT-II) and the anhydrous pollucite-related triclinic phase (anh-Cs-POL), and finally to the hexacelsian-related phase (Cs-HEX) which forms above 3.7 GPa and at 180 °C. Rietveld structural refinements reveal that the recovered hexacelsian-like phase is ca. 8.4% less dense than the original Cs-NAT-I.

Experimental Section

- Sample preparation and synchrotron X-ray powder diffraction

The preparation of Cs-exchanged natrolite (Cs-NAT-I) and its dehydrated form (deh-Cs-NAT) is described in detail by Lee et al. (2010) and Lee et al. (2011). *In situ* high-pressure synchrotron X-ray powder diffraction was performed using a Merrill-Bassett type diamond-anvil cell (DAC) at the X14A beamline at the National Synchrotron Light Source (NSLS) at Brookhaven National Laboratory (BNL). The primary white beam from a bending magnet was horizontally monochromatized by Si (111) focusing double crystals to produce monochromatic X-ray with wavelength of 0.77455 Å and 0.77485 Å

[leave only one wavelength used!]. The powder sample was loaded into a 410μm diameter - 110μm thick sample chamber in a pre-indented stainless steel gasket. A few small ruby spheres were used as *in situ* pressure markers inside the sample chamber. Distilled water was used as a pore-penetrating pressure-transmitting medium (PTM). After applying the PTM to the sample, the DAC was quickly sealed to the first measured pressure point. The pressure at the sample was measured by detecting R_1 emission line of the included ruby spheres in the DAC (Mao et al. 1986). Pressure was increased up to 4.32 GPa at step intervals of ca. 0.25 GPa. *Ex situ* heat treatment was occasionally applied by placing the DAC inside an oven for a few hours to induce hydrostatic conditions of the PTM at respective pressures. The *in situ* pressure and *ex situ* heat treatment sequences are summarized in Table 1 along with the resulting changes in the unit-cell volume and calculated density.

- Rietveld structure refinement

Structural refinements of the recovered hexacelsian-like phase, Cs-HEX, formed at 3.7 GPa after heating at 180 °C were performed by Rietveld methods using GSAS and EXPGUI (Larson and Von Dreele 1986; Toby 2001). The background curve was fitted with a Chebyshev polynomial. The pseudo-Voigt profile function proposed by Thompson et al. (1987) was used to fit the observed peaks. The starting framework model used was that of the Ba-hexacelcian ($P6_3/mcm$) by Kremenovic et al. (2003). The tetrahedral site (T-site) was assumed to be statistically occupied by Si and Al atoms. An inspection of the difference-Fourier map of the electron density suggested that the Cs was located at the extra-framework 2*b* (0,0,0) site. The refined occupancy of the Cs cation was then used to

fix the Al occupancy at the disordered T-site. Geometrical soft restraints were applied on the disordered T-site based on the fixed occupancies of $Si_{0.81}$ and $Al_{0.19}$; T-O and O-O inter-atomic distances of the tetrahedra were restrained to target values of 1.635 ± 0.001 Å, and 2.669 ± 0.005 Å, respectively. To reduce the number of parameters, all the atoms were modeled with one isotropic displacement parameters (U_{iso}). Preferred orientation along [00l] directions were taken into account and corrected for. Scanning transmission electron microscopy imaging revealed that the crystallites are thin platelets perpendicular to the [001] direction (see Figure 5). Reflections with d-spacing along the [001] direction are therefore statistically under-sampled in a powder experiment and appropriate preferred orientation corrections need to be applied. Preferred orientation function of xxx (indicate which function you used and add that reference) was used and the values were refined to xxx and xxx (add these numbers). In the final stage of the refinements, the weights of the soft restraints were reduced, which did not result in any significant changes of the inter-atomic distances. The final convergence of the refinement was achieved by varying simultaneously all background and profile parameters, preferred orientation parameters, scale factor, lattice constants, 2θ zero, and the atomic positional and displacement parameters. The results of the final refined models are summarized in Tables 2, 3 and 4.

- Imaging using High Angle Annular Dark Field Scanning Transmission Electron Microscopy

Scanning transmission electron microscopy was used to image the atomic arrangements of the recovered Cs-HEX particles using a JEOL 2100F 200kV FEG-STEM/TEM

equipped with a CEOS Cs corrector on the illumination system. High angle annular dark-field STEM images were acquired on a Fischione Model 3000 HAADF detector with a camera length such that the inner cut-off angle of the detector was 75 mrad. The acquired real space images are shown in Fig. 5.

Results and Discussion

The changes in the synchrotron X-ray powder diffracttion patterns at respective pressures and temperatures show successive transformations from deh-Cs-NAT to Cs-HEX (Fig. 1). Above 0.5 GPa and 100 °C, deh-Cs-NAT (*i.e.,* $Cs_{16}Al_{16}Si_{24}O_{80}$) transform to the hydrated phase, Cs-NAT-II (*i.e.*, $Cs_{16}Al_{16}Si_{24}O_{80}\cdot 16H_2O$) *via* pressure-induced hydration. The insertion of H_2O molecules from the PTM into the natrolite channels causes the expansion of the unit-cell volume by ca. 13.9% (Table 1, Fig. 2). As a result, the density of Cs-NAT-II decreases by c.a. 6.5% compared to deh-Cs-NAT at 0.5 GPa. In Cs-NAT-II, the Cs^+ cations migrate towards the middle of the channel as the H_2O molecules occupy the wall sites of the channel (Fig. 3). The amount of H_2O molecules inserted under pressure is 16 per $80O_f$, which is the same as in the original Cs-exchanged natrolite (Seoung et al. 2013). The Cs^+-H_2O cluster in Cs-NAT-II are in an ordered arrangement with fully occupied cation and H_2O sites, unlike the statistically-distributed model in the original Cs-exchanged natrolite. As the DAC is annealed at 145 °C and 1.5 GPa, Cs-NAT-II transforms partially to a triclinic H_2O-free pollucite-like phase $Cs_{16}Al_{16}Si_{32}O_{96}$ (anh-Cs-POL). This leads to the contraction of the unit-cell volume by ca. 15.6% per $80O_f$ (Table 1, Fig. 2). While the initial pressure-induced hydration is

topotactic with respect to the framework and facilitated by an opening of the pores due to the auxetic properties of this framework (Grima et 1l 2007, Kremleva et al 2013, Seoung et al 2013), the dehydration at 0.5 GPa and 100 °C leads to a reconstruction of the framework accompanied by Cs and Al leaching.

Further increase in pressure to 2.6 GPa leads to a complete conversion of Cs-NAT-II into anh-Cs-POL persisting up to 3.7 GPa. After heating at 180°C, anh-Cs-POL transforms to a new hexagonal phase, with a hexacelsian-like framework in $P6_3/mcm$. This hexacelsian-like phase, *i.e.* Cs-HEX, was observed up to the final pressure of 4.3 GPa and is recovered after pressure release (Figs. 1 and 2). The unit-cell volume of the recovered Cs-HEX is ca. 6.7% smaller than that of the starting deh-Cs-NAT per $80O_f$ and therefore about 9.0% smaller than that of the original Cs-NAT-I, respectively, at ambient conditions. The overall pressure- and temperature-induced transformations are illustrated in Fig. 3.

The structural model of Cs-HEX was derived from Rietveld structural refinements using synchrotron X-ray powder diffraction data collected under pressure and after pressure release (Table 2, 3 and 4; Fig. 4). Similar to the Ba-hexacelsian structure, the refined structure of Cs-HEX is composed of double sheets of disordered Si/Al tetrahedra on the plane perpendicular to the *c*-axis. Each double sheet consists of upward- and downward-oriented TO_4 tetrahedral sub-layers bridged by O1 oxygen hinges with T-O1-T angles of 180° (Table 4). Within each sub-layer, O2 oxygen hinges bridge the individual tetrahedra with T-O2-T angle in the range between 140.3(4)° and 141.4(2)°. This is larger than observed in the Ba-hexacelsian structure (Fig. 4). Cs-HEX contains Cs^+ cations located at the 2*b* (0,0,0) sites between the double sheets of

tetrahedra, with interlayer distances in the range between 3.306(6) Å and 3.897(11) Å. In contrast to fully occupied of Ba^{2+} sites in Ba-hexacelsian, the refined occupancy of Cs^{+} cation is 0.773(6) which results to 1.5(1) Cs atoms per unit-cell. In fact, when refined, the Al/Si ratio converges to ca. 0.24(1) or 1.5(1) Al atoms per unit-cell, which matches the amount of Cs^{+} cations needed for electro-neutrality. We therefore propose the chemical formula of Cs-HEX to be $Cs_{1.55}Al_{1.55}Si_{6.45}O_{16}$. The decrease in the Al/Si ratio from the starting phase, *i.e.* 0.67 in Cs-natrolite, could be due to a phase separation and the formation of minor, yet uncharacterized and highly disordered phases of aluminum and cesium, which might be the reason for broad humps observed in the diffraction patterns (Fig. 1). In Cs-HEX, the Cs^{+} cations are coordinated by 12 oxygen atoms, *i.e.* six O2 atoms from the upper and the other six from the bottom layer with interatomic distances in the range between 3.326(8) Å and 3.311(8) Å (Fig. 4). In Ba-hexacelsian, Ba^{2+} is hexa-coordinated by three O2 oxygen atoms from the upper and the bottom layer each with interatomic distance of 3.052 Å and hexa-coordination at 3.151 Å. To a first approximation the contrast of atomic columns imaged using HAADF-STEM varies with Z^2, Z being the atomic number of the element. The unique Cs^{+} arrangement in the Cs-HEX structure is observed in HAADF-STEM real space images measured from recovered Cs-HEX particles as shown in Fig. 5 where the bright spots indicate the position of the Cs^{+} ions. Having both Ba- and Cs-HEX structurally well characterized might help to model chemical and structural changes occurring during the decay of $^{137}Cs^{+}$ under β- and γ- emissions to $^{137}Ba^{2+}$, changing the cation valence and ionic radius. Further experimental findings in this field have been reported by Jiang and Van Ginhoven (2012).

Implications

The experimental findings of this study open a new window on the behavior of Cs-bearing open-framework aluminosilicates in response to pressure and temperature. A *P/T*-induced densification process was observed from a Cs-bearing zeolite (with NAT topology) to a Cs-hexacelsian, through a series of phase transformations toward a final product which survives at room conditions. The mechanisms of *P/T*-induced densification of crystalline materials are the basis to understand the mineralogical processes under extreme conditions, but in this case the main implications of the experimental findings extend to nuclear technology. Pollucite-like materials have been considered among the most stable Cs-bearing aluminosilicates for the inertization of Cs-rich nuclear wastes. The high Cs-content of approximately 40 weight% in pollucite exceeds that of any Cs-containing glass ceramics or zeolites (Donald et al. 1997). Furthermore, the Cs leaching rate indicates that this material might be used for long term storage of ^{137}Cs at ambient conditions (Yanagisawa et al. 1987). We deemed it important to further explore the high-temperature and high-pressure chemistry of the new pollucite-related phase obtained by the *P/T*-treatment of Cs-natrolite, in order to assess processes which might affect its use. We show here that by increasing pressure and temperature another dense phase exists, namely Cs-hexacelsian which contains less Cs per formula unit than pollucite. The reconstructive phase transition from the anhydrous triclinic pollucite phase to Cs-hexacelsian results in the precipitation of Cs^+ and $Al^{3+}$and therefore these pressure and temperature conditions need to be avoided if the storage of radioactive Cs^+ is targeted.

Acknowledgments

This work was supported by the Global Research Laboratory Program of the Korean Ministry of Science, ICT and Planning (MSIP). Experiments at PAL were supported in part by the MSIP and Pohang University of Science and Technology (POSTECH). Research carried out in part at the NSLS at BNL is supported by the U.S. Department of Energy, Office of Basic Energy Sciences. The authors thank Dr. Hyun Hwi Lee at PAL and Dr. Jianming Bai at BNL for their supports on the synchrotron experiments. GDG acknowledges the Italian Ministry of Education, MIUR-Project: "Futuro in Ricerca 2012 - ImPACT- RBFR12CLQD".

References

Baur, W.H., Kassner, D., Kim, C.-H., Sieber, N.H.W. (1990) Flexibility and distortion of the framework of natrolite: crystal structures of ion-exchanged natrolites. European Journal of Mineralogy, 2, 761-769.

Gatta, G.D. (2005) A comparative study of fibrous zeolites under pressure. European Journal of Mineralogy, 17, 411-421.

Gatta, G.D. and Lee, Y. (2014) Zeolites at high pressure: A review. Mineralogical Magazine, 78, 267-291.

Gatta, G.D., Rinaldi, R., McIntyre, G.J., Nénert, G., Bellatreccia, F., Guastoni, A., Della Ventura G. (2009a) On the crystal structure and crystal chemistry of pollucite, $(Cs,Na)_{16}Al_{16}Si_{32}O_{96}\cdot nH_2O$: a natural microporous material of interest in nuclear

technology. American Mineralogist, 94, 1560-1568.

Gatta, G.D., Rotiroti, N., Boffa Ballaran, T., Sanchez-Valle, C., Pavese, A. (2009b) Elastic behavior and phase-stability of pollucite, a potential host for nuclear waste. American Mineralogist, 94, 1137-1143.

Grima, J.N., Gatt, R., Zammit, V., Williams, J.J., Evans, K.E., Alderson, A., Walton, R. I. (2007) Natrolite: A zeolite with negative Poisson's ratios. Journal of Applied Physics, 101, 086102

Jiang, W. and Van Ginhoven, R.M. (2012) Chemical and Charge Im-balance Induced by Radionuclide Decay: Effects on Waste Form Structure. Pacific Northwest National Laboratory (PNNL), Richland, WA (US), Environmental Molecular Sciences Laboratory (EMSL) PNNL-20312-3

Klaproth, M.H. (1803) Ges. Naturforsch. Freunde Berlin, Neue Schrifl, 4, 243-248.

Kremenović, A., Colomban, P., Piriou, B., Massiot, D., Florian P. (2003) Structural and spectroscopic characterization of the quenched hexacelsian. The Journal of Physics and Chemistry of Solids, 64(11), 2253-2268.

Kremleva, A., Vogt, T., Rösch, N. (2013) Monovalent cation-exchanged natrolites and their behavior under pressure. A computational study. Journal of Physical Chemistry C, 117(37), 19020-19030.

Larson, A. and Von Dreele, R.B. (1986) GSAS : General Structure Analysis System. Los Alamos National Laboratory, New Mexico, Report LAUR, 86-748.

Lee, Y., Hriljac, J.A., Parise, J. B., Vogt, T. (2005) Pressure-induced stabilization of ordered paranatrolite: A new insight into the paranatrolite controversy. American

Mineralogist, 90(1), 252-257.

Lee, Y., Seoung, D., Jang, Y.N., Vogt, T., Lee, Y. (2013) Role of Cation–Water Disorder during Cation Exchange in Small-Pore Zeolite Sodium Natrolite. The Journal of Physical Chemistry C, 117(31), 16119-16126.

Lee, Y., Lee, Y., Seoung, D. (2010) Natrolite may not be a “soda-stone” anymore: Structural study of fully K-, Rb-, and Cs-exchanged natrolite. American Mineralogist, 95(11-12), 1636-1641.

Lee, Y., Seoung, D., Lee, Y. (2011) Natrolite is not a “soda-stone” anymore: Structural study of alkali (Li^{+}), alkaline-earth (Ca^{2+}, Sr^{2+}, Ba^{2+}) and heavy metal (Cd^{2+}, Pb^{2+}, Ag^{+}) cation-exchanged natrolites. American Mineralogist, 96(11-12), 1718-1724.

Pauling, L. (1930) The structure of some sodium and calcium aluminosilicates. Proceedings of the National Academy of Sciences of the United States of America, 16(7), 453-459.

Sanchez-Valle, C., Chi-Hong, C., Gatta, G.D. (2010) Single-crystal elastic properties of $(Cs,Na)AlSi_2O_6 \bullet H_2O$ pollucite: with potential use for long-term storage of Cs radioisotopes. Journal of Applied Physics, 108, 093509 (1-7).

Seoung, D., Lee, Y., Kao, C.C., Vogt, T., Lee, Y. (2013) Super-hydrated zeolites: Pressure-induced hydration in natrolites. Chemistry-A European Journal, 19(33), 10876-10883.

Taylor, W.H., Meek, C.A., and Jackson, W.W. (1933) The structures of the fibrous zeolites. Zeitschrift für Kristallographie, 84(1), 373-398.

Thompson, P., Cox, D.E., and Hastings, J.B. (1987) Rietveld refinement of Debye-Scherrer synchrotron X-ray data from Al_2O_3. Journal of Applied Crystallography,

20(2), 79-83.

Toby, B.H. (2001) EXPGUI, a graphical user interface for GSAS. Journal of Applied Crystallography, 34(2), 210-213.

Yanagisawa, K., Nishioka, M., Yamasaki, N.J. (1987) Immobilization of cesium into Pollucite structure by hydrothermal hot-pressing. Journal of Nuclear Science and Technology, 24(1), 51-60.

Figure Captions

Figure 1. Synchrotron X-ray powder diffraction patterns of dehy-Cs-NAT at ambient (bottom) and under increasing pressure conditions. Temperatures indicate *ex situ* heating before the measurement. Top pattern shows Rietveld fit of Cs-HEX with difference curve (blue line) between the observed (black crosses) and calculated (red line) patterns.

Figure 2. Pressure- and heat-induced changes in the unit-cell volumes, normalized to 80 framework oxygen atoms ($80O_f$) of dehydrated Cs-exchanged natrolite (deh-Cs-NAT), ordered hydrated natrolite (Cs-NAT-II), H_2O-free pollucite-like phase (anh-Cs-POL), and the hexacelsian-like phase (Cs-HEX).

Figure 3. Polyhedral representations of the successive transformations from the dehydrated Cs-exchanged natrolite (deh-Cs-NAT), the ordered hydrated natrolite (Cs-NAT-II), the H_2O-free pollucite-like phase (anh-Cs-POL), and to the hexacelsian-like phase (Cs-HEX). Red and yellow circles represent H_2O molecules and Cs^+ extra-framework cations, respectively. Two-toned polyhedra in the natrolite framework illustrate the ordered arrangements of the Si- and Al-tetrahedra.

Figure 4. Crystal structure of the hexacelsian-like phase (Cs-HEX) com-pared to the Ba-hexacelsian by Kremenovic et al. (2003). Upper and lower figures are views along and perpendicular to the c-axis, respectively. Cation-to-oxygen coordination distances are illustrated with two separate bars for long- and short-bonds.

Figure 5. HAADF-STEM images from a recovered Cs-HEX particle viewed down [001]. A tetrahedral representation of the refined Cs-HEX structure is overlain on the experimental HAADF-STEM image to show the match between the Z-contrast and the distribution of the Cs^+ extra-framework cations in the model.

Table 1. Pressure- and heat-induced changes in the unit-cell volume, normalized to 80 framework oxygen atoms ($80O_f$) from the dehydrated Cs-exchanged natrolite (deh-Cs-NAT), the ordered hydrated natrolite (Cs-NAT-II), the H_2O-free pollucite-like phase (anh-Cs-POL), and to the hexacelsian-like phase (Cs-HEX).

Phase	Pressure (GPa)	Temperature treatment (°C)	Volume per $80O_f$ ($Å^3$)
deh-Cs-NAT	0.0001		2235.6(3)
	0.5(1)		2197.5(3)
Cs-NAT-II	0.5(1)	100	2503.0(2)
	0.8(1)		2475.5(3)
	0.8(1)	120	2473.3(2)
	1.3(1)		2432.7(2)
	1.3(1)	140	2437.9(2)
	1.5(1)		2416.4(1)
	1.5(1)	145	2413.4(2)
	2.0(1)		2393.6(2)
anh-Cs-POL	1.5(1)	145	2039.3(2)
	2.0(1)		2018.2(2)
	2.6(1)		1992.2(2)
	2.6(1)	165	1988.3(2)
	3.7(1)		1942.3(2)
Cs-HEX	3.7(1)	180	1907.2(1)
	4.3(1)		1894.3(5)
	4.3(1)	190	1880.5(2)
	1.0(1)		2028.9(2)
	0		2085.6(2)

Table 2. Crystal data and details pertaining to the structure refinements of the hexacelsian-like phase (Cs-HEX) compared to those of the Ba-hexacelsian by Kremenovic et al. (2003).

	Cs-HEX (released)	Cs-HEX (3.7 GPa, 180 °C)	Cs-HEX (4.3 GPa, 190 °C)	Ba-HEX
Unit-cell formula		$Cs_{1.547}Al_{1.548}Si_{6.452}O_{16}$		$Ba_2Al_4Si_4O_{16}$
Formula weight		684.55		750.91
Space group		$P6_3/mcm$		$P6_3/mcm$
Unit-cell dimension (Å)	a = 5.3731(2) c = 16.6834(8)	a = 5.3275(1) c = 15.5180(5)	a = 5.3172(2) c = 15.3606(7)	a = 5.2920(4) c = 15.557(2)
Unit-cell Volume(Å^3)	417.12(4)	381.43(2)	376.10(3)	377.308
Calculated density(g/cm^3)	2.725	2.980	3.022	3.306
Parameters reduced χ^2	15.87	3.563	3.533	
R_{wp}(%)	5.42	6.72	7.17	

Table 3. Refined atomic positional, occupancy, and displacement parameters of the hexacelsian-like phase (Cs-HEX) compared to those of the Ba-hexacelsian by Kremenovic et al. (2003). Estimated standard deviations are in parenthesis.

		Cs-HEX (release)	Cs-HEX (3.7 GPa, 180 °C)	Cs-HEX (4.3 GPa, 190 °C)			Ba-HEX
T 8*h*	*x*	1/3	1/3	1/3	T 8*h*	*x*	1/3
	y	2/3	2/3	2/3		*y*	2/3
	z	0.150(1)	0.145(1)	0.144(1)		*z*	0.145(2)
	occu. Al/Si	0.1935 / 0.8065	0.1935 / 0.8065	0.1935 / 0.8065		*occu.*	0.5/0.5
	U_{iso}	0.015(1)	0.015	0.015		U_{iso}	0.01140
O1 4*c*	*x*	1/3	1/3	1/3	O1 4*c*	*x*	1/3
	y	2/3	2/3	2/3		*y*	2/3
	z	1/4	1/4	1/4		*z*	1/4
	occu.	1.0	1.0	1.0		*occu.*	1.0
	U_{iso}	0.015(1)	0.015	0.015		U_{iso}	0.01267
O2 12*k*	*x*	0.498(2)	0.489(1)	0.498(1)	O2 12*k*	*x*	0.489(3)
	y	0	0	0		*y*	0
	z	0.117(1)	0.110(1)	0.108(1)		*z*	0.104(2)
	occu.	1.0	1.0	1.0		*occu.*	1.0
	U_{iso}	0.015(1)	0.015	0.015		U_{iso}	0.04559
Cs 2*b*	*x*	0	0	0	Ba 2*b*	*x*	0
	y	0	0	0		*y*	0
	z	0	0	0		*z*	0
	occu.	0.773(6)	0.773	0.773		*occu.*	1
	U_{iso}	0.015(1)	0.015	0.015		U_{iso}	0.02026

Table 4. Selected interatomic distances (Å) and angle (o) of the hexacelsian-like phase (Cs-HEX) compared to those of the Ba-hexacelsian by Kremenovic et al. (2003). Estimated standard deviations are in parenthesis.

	Cs-HEX (released)	Cs-HEX (3.7 GPa, 180 °C)	Cs-HEX (4.3 GPa, 190 °C)		Ba-HEX
T-O1	1.663(2)	1.634(1)	1.635(1)	T-O1	1.642
T-O2	1.649(2) × 3	1.630 (1) × 3	1.631(1) × 3	T-O2	1.652 × 3
O1-O2	2.710(4)	2.661(3)	2.672(3)	O1-O2	2.738
O2-O2	2.687(1)	2.666(1)	2.659(1)	O2-O2	2.678
Cs-O2	3.326(8) × 6 3.311(8) × 6	3.215(6) × 6 3.115(5) × 6	3.141(4) × 6 3.120(4) × 6	Ba-O2	3.052 × 6 3.151 × 6
T-O1-T	180.0	180.0	180.0	T-O1-T	180
T-O2-T	140.3(4)	141.4(2)	140.4(2)	T-O2-T	135
Distance between T-layer	3.897(11)	3.421(7)	3.306(6)	Distance between T-layer	3.238

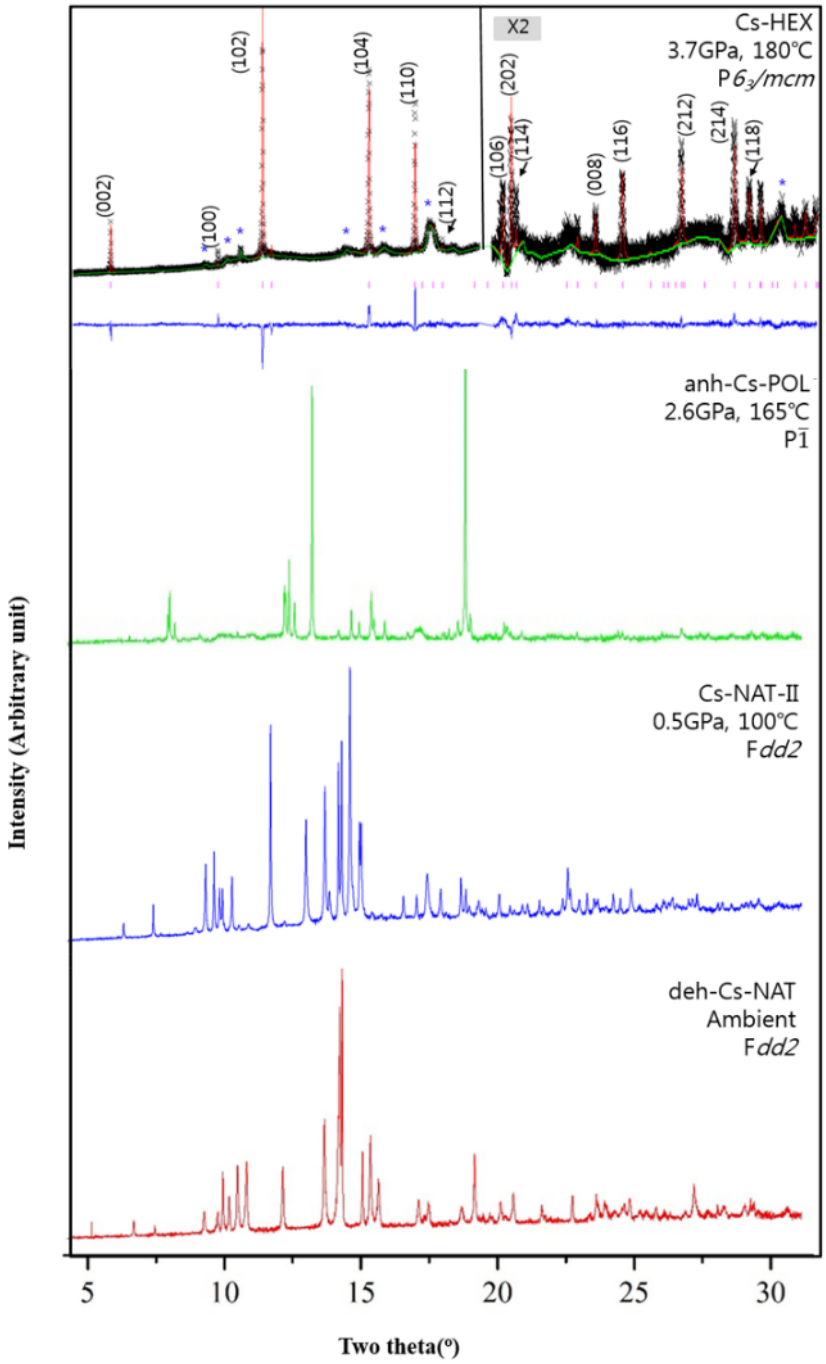
Cs-HEX
3.7GPa, 180°C
P6₃/mcm
X2
(002)
(100)
(102)
(104)
(110)
(112)
(106)
(202)
(114)
(008)
(116)
(212)
(214)
(118)
anh-Cs-POL
2.6GPa, 165°C
PĪ
Cs-NAT-II
0.5GPa, 100°C
Fdd2
deh-Cs-NAT
Ambient
Fdd2
Intensity (Arbitrary unit)
5
10
15
20
25
30
Two theta(°)

Figure 1

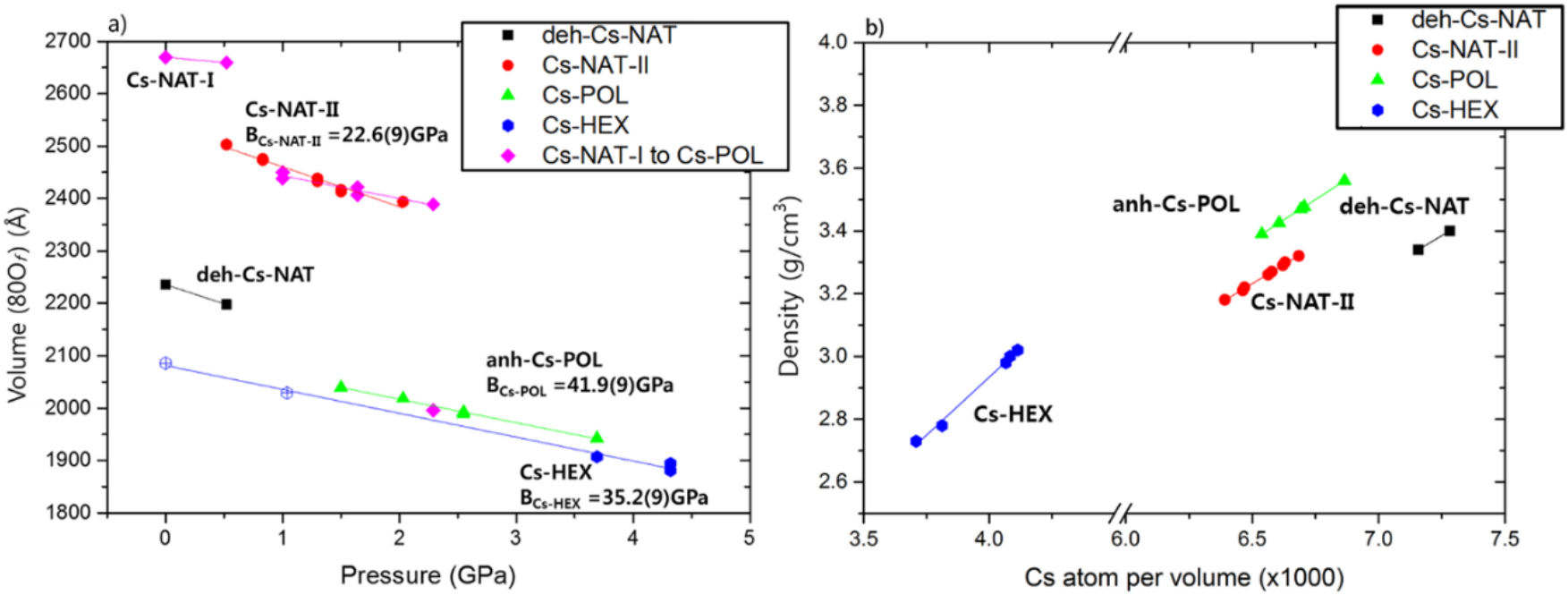
a)
Cs-NAT-I
Cs-NAT-II
$B_{Cs\text{-}NAT\text{-}II}$ =22.6(9)GPa
deh-Cs-NAT
anh-Cs-POL
$B_{Cs\text{-}POL}$ =41.9(9)GPa
Cs-HEX
$B_{Cs\text{-}HEX}$ =35.2(9)GPa
deh-Cs-NAT
Cs-NAT-II
Cs-POL
Cs-HEX
Cs-NAT-I to Cs-POL
Volume (80O$_h$) (Å)
Pressure (GPa)
b)
anh-Cs-POL
deh-Cs-NAT
Cs-NAT-II
Cs-HEX
deh-Cs-NAT
Cs-NAT-II
Cs-POL
Cs-HEX
Density (g/cm^3)
Cs atom per volume (x1000)

Figure 2

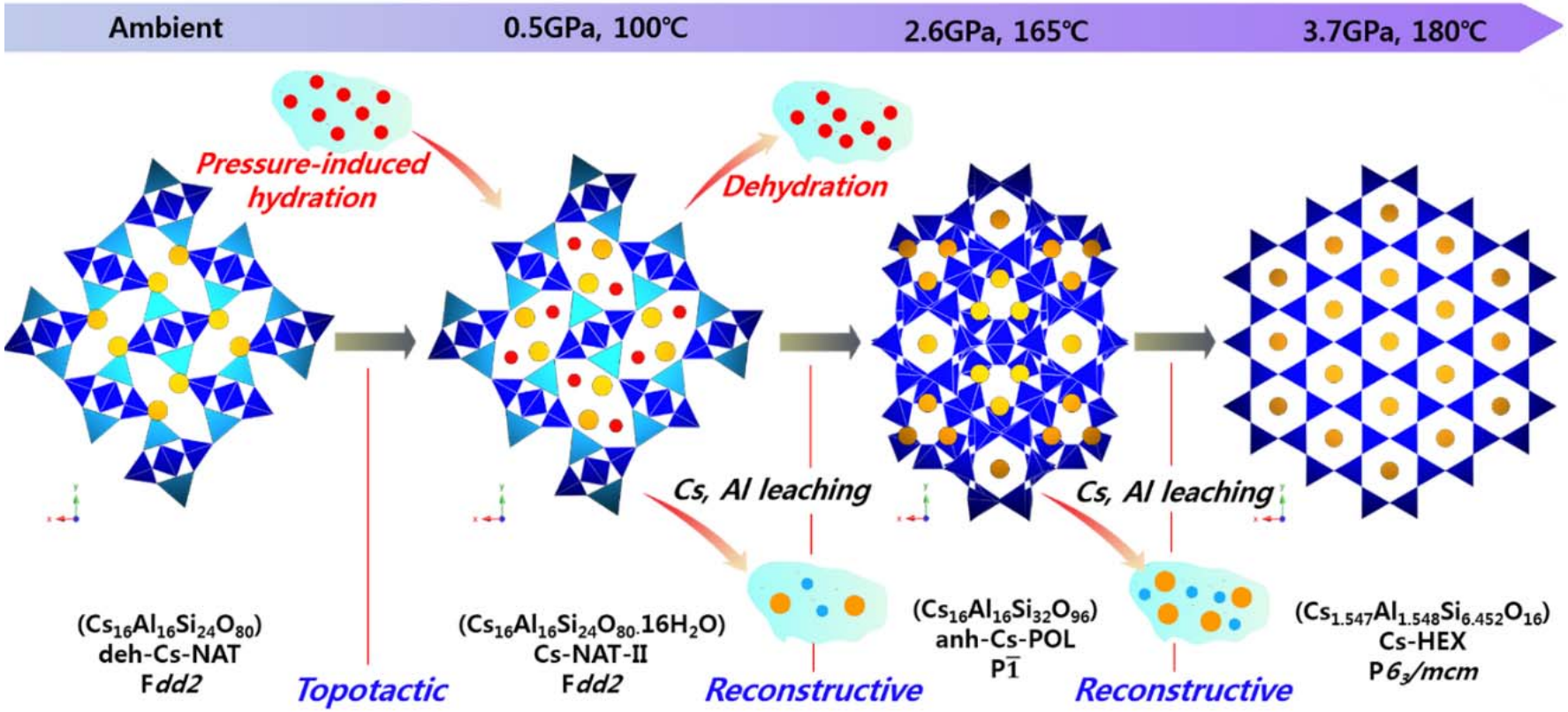
Ambient
0.5GPa, 100℃
2.6GPa, 165℃
3.7GPa, 180℃
Pressure-induced hydration
Dehydration
Cs, Al leaching
Cs, Al leaching
(Cs16Al16Si24O80)
deh-Cs-NAT
Fdd2
Topotactic
(Cs16Al16Si24O80.16H2O)
Cs-NAT-II
Fdd2
Reconstructive
(Cs16Al16Si32O96)
anh-Cs-POL
P1̄
Reconstructive
(Cs1.547Al1.548Si6.452O16)
Cs-HEX
P63/mcm

Figure 3

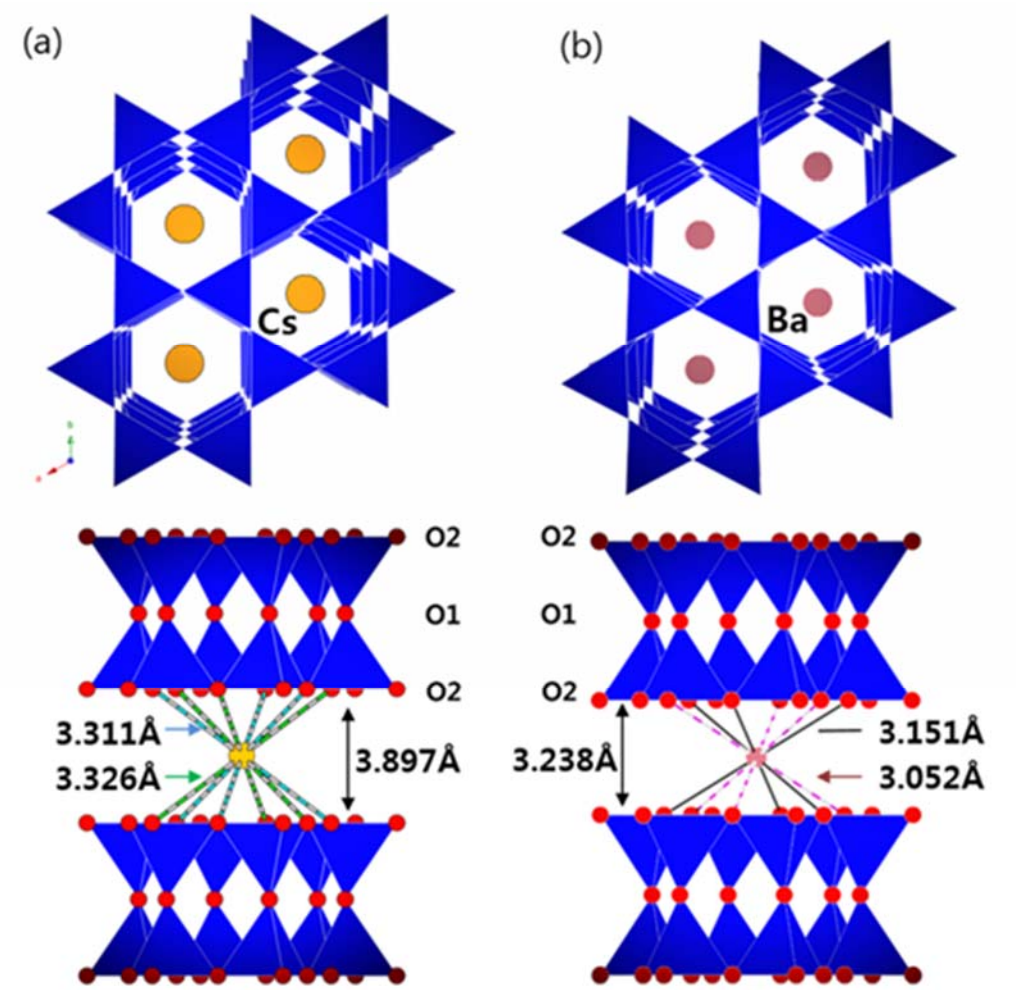

Figure 4

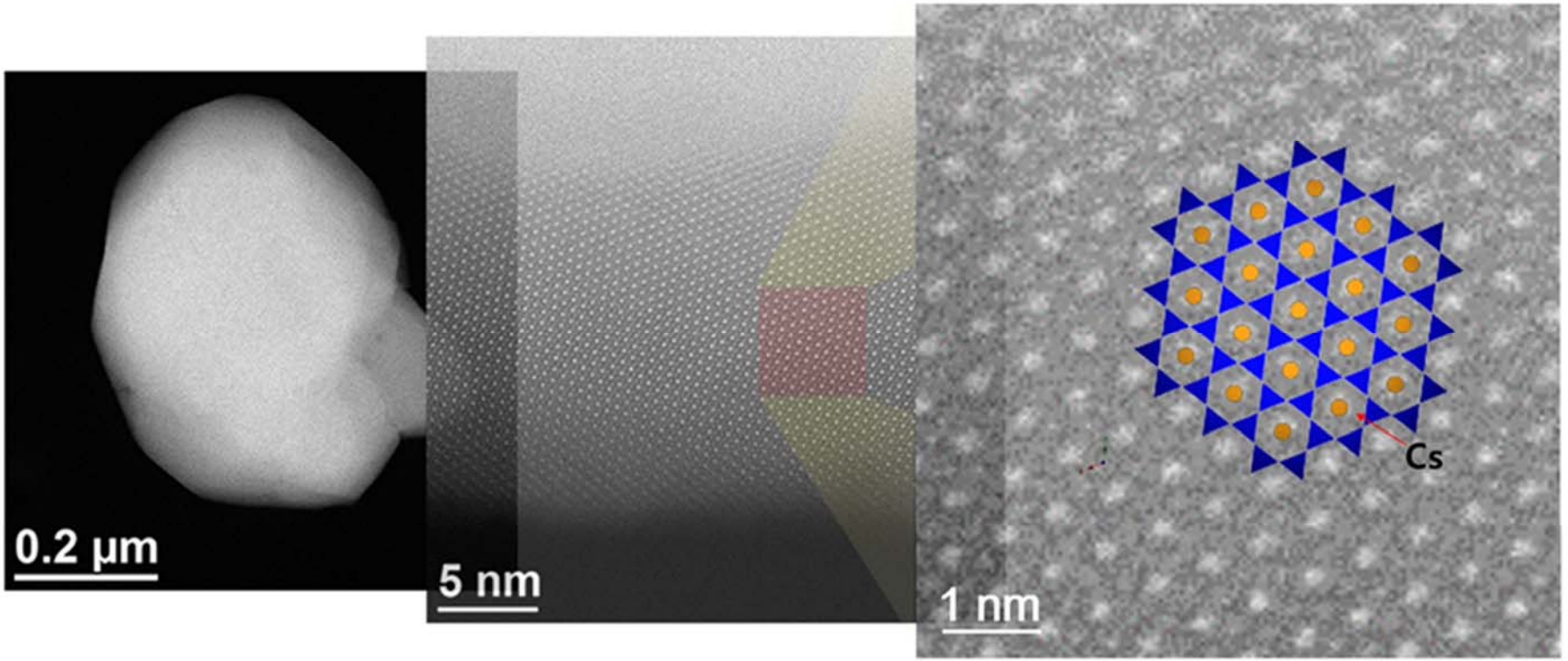

Figure 5